NASA

Technical Memorandum 83951

Low-Level Water Vapor Fields From the VISSR Atmospheric Sounder (VAS) "Split Window" Channels at 11 and 12 Microns

D. Chesters, L. Uccellini, and W. Robinson

MAY 7, 1982

National Aeronautics and
Space Administration

Goddard Space Flight Center
Greenbelt, Maryland 20771

TM 83951

LOW-LEVEL WATER VAPOR FIELDS FROM THE VISSR ATMOSPHERIC SOUNDER (VAS) "SPLIT WINDOW" CHANNELS AT 11 AND 12 MICRONS

by

Dennis Chesters and Louis W. Uccellini
Goddard Laboratory for Atmospheric Sciences
NASA/Goddard Space Flight Center
Greenbelt, Maryland 20771

and

Wayne Robinson
Computer Sciences Corporation
Silver Spring, Maryland 20910
Goddard Laboratory for Atmospheric Sciences
NASA/Goddard Space Flight Center
Greenbelt, Maryland 20771

May 7, 1982

GODDARD SPACE FLIGHT CENTER
Greenbelt, Maryland 20771

LOW-LEVEL WATER VAPOR FIELDS FROM THE VISSR ATMOSPHERIC SOUNDER (VAS) "SPLIT WINDOW" CHANNELS AT 11 AND 12 MICRONS

D. Chesters, L. Uccellini, and W. Robinson

ABSTRACT

A series of high-resolution water vapor fields are derived from the 11 and 12 μm channels of the VISSR Atmospheric Sounder (VAS) on GOES-5. The low-level tropospheric moisture content is separated from the surface and atmospheric radiances by using the differential absorption across the "split window" along with the average air temperature from imbedded radiosondes. Fields of precipitable water (gm cm^{-2}) are presented in a time sequence of five false color images taken over the United States at 3-hour intervals on 13 July 1981. Vivid subsynoptic and mesoscale patterns evolve at 15 km horizontal resolution over the 12-hour observing period. Convective cloud formations develop from several areas of enhanced low-level water vapor, especially where the vertical water vapor gradient (inferred from overlays of high-level moisture patterns found in the corresponding VAS 6.7 μm channel) is relatively strong. Independent verification at radiosonde sites indicates fairly good absolute accuracy (±0.67 gm cm^{-2} from 1.8 to 5.3 gm cm^{-2}), and the spatial and temporal continuity of the water vapor features indicates very good relative accuracy. Residual errors are dominated by radiometer noise and unresolved clouds. The algorithm can produce quality controlled images of the vertically integrated water vapor in relatively cloud free areas from real-time VAS data, closely monitoring the development of regional moisture features which would remain otherwise undetected and/or unresolved.

CONTENTS

TABLES

ILLUSTRATIONS

LOW-LEVEL WATER VAPOR FIELDS FROM THE VISSR ATMOSPHERIC SOUNDER (VAS) "SPLIT WINDOW" CHANNELS AT 11 AND 12 MICRONS

1.0 INTRODUCTION

1.1 Motivation

The VISSR Atmospheric Sounder (VAS) is the thermal infrared radiometer now operating on the Geostationary Operational Environmental Satellite (GOES). The VAS instrument is an improved version of the previous imager on the GOES, with eleven infrared channels added to the 11 μm window and visible detectors. Radiometric quality has been upgraded as well, with ten bit precision in place of eight, $\pm 1.5^{\circ}$K calibration accuracy instead of $\pm 3.0^{\circ}$K, and six infrared detectors instead of one. The VAS is intended to exploit its geosynchronous station by observing the development of mesoscale temperature and water vapor fields with frequent multi-channel images at 15 km horizontal resolution (nadir view) in the spectral windows and molecular absorption bands of the earth's thermal infrared spectrum (Suomi, et al., 1971). In particular, the pair of channels at 11 and 12 μm are designed to use the differential water vapor absorption across this part of the spectrum in order to estimate the water vapor absorption along the line of sight. The two channels are called a "split window" because they use the difference in brightness at two adjacent bandpasses in order to separate the atmospheric and surface radiance contributions. The VAS split window is used in a simple algorithm to produce false color images of the water vapor content of the lower troposphere. This bulk water vapor estimate is certainly not as sophisticated as a water vapor *profile* retrieval using all of the VAS channels and human quality control. Rather, it is a real-time algorithm for making high-resolution mesoscale images from only two channels which display the horizontal low-level water vapor distribution in relatively clear air.

For the near future, NOAA will operate VAS with minimal impact upon the pre-established community of VISSR (visible and 11 μm infrared) data users. The additional VAS detectors make

it possible to deliver the 6.7 and 12 μm radiances simultaneously along with the conventional VISSR data to any ground station with VAS data handling capability. Consequently, these three VAS infrared channels can be used for routine mesoscale monitoring of water vapor fields. These expectations have motivated the development of an algorithm which can automatically produce real-time water vapor estimates from these channels alone.

1.2 Background

In general, atmospheric water vapor sounding from satellite radiances is more difficult than temperature sounding because:

a. Vertical water vapor structures are often not resolved by the broad vertical extent of the passive radiometer response functions.

b. Most of the precipitable water along a line of sight is concentrated in the air just above a bright background of highly variable topography, emissivity and skin temperature.

c. The radiance contribution from the atmosphere is a combination of both the air temperature and the water vapor content.

Nevertheless, some quantitative information about the atmospheric water vapor can be retrieved from passive thermal infrared satellite data.

For example, recent case studies of mesoscale water vapor retrievals with the High-Resolution Infrared Sounder (HIRS) over the Texas–Oklahoma area were able to display dryline features down to the 30 km horizontal resolution of that instrument (Hillger and Vonder Haar, 1981). These HIRS analyses could only determine the relative horizontal structure of the water vapor features, and not their absolute magnitudes. Similar error patterns have also been found in the operational satellite *temperature* soundings: there are larger errors near the surface, biases in areas of unusual topography or clouds, and systematically underestimated horizontal gradients. Such problems have been found both over ocean (Phillips, et al., 1979) and over land (Schlatter, 1981). Likewise, *simulated* case studies of VAS water vapor retrievals within pre-convective environments have shown a pattern of good relative gradient determination, but poor absolute accuracy (Chesters, et al.,

1982). In particular, the VAS simulations showed a poor linear correlation between the split window brightness difference and the low-level mixing ratio, due to the general problems with water vapor retrievals.

The first VAS instrument was launched on GOES-4 in the autumn of 1980, and it is currently operational at 135°W. Initial experience with the VAS data indicated that the instrument is a relatively stable, somewhat biased radiometer (Menzel, et al., 1981). Temperature and water vapor profiles have been retrieved by using careful radiometric corrections and a physical retrieval method at hand-picked, clear fields-of-view (Smith, et al., 1981). The VAS on GOES-4 has also been used as a mesoscale temperature and water vapor field interpolator between radiosonde stations (Chesters, et al., 1981). Subsynoptic low-level water vapor features definitely appear in objective analyses of the VAS soundings from both retrieval methods. Mesoscale features derived from VAS cannot be verified with the relatively coarse, infrequent radiosonde network. In this sense, VAS is the *only* available source of frequent, quantitative, high-resolution atmospheric data for the United States. The data used in this paper are from the second VAS instrument, launched on GOES-5 in the spring of 1981. The data were acquired during demonstration and testing of the VAS Processor at NASA/GSFC in the summer of 1981, just before GOES-5 was moved from its post-launch station at 85°W to its current operational station at 75°W.

1.3 Outline

This paper describes a fast, simple algorithm for estimating the low-level precipitable water in clear air from the VAS split window channels at 11 and 12 μm. The low-level moisture algorithm presented in Section 2 is based on a physical model for radiation transfer through a single thick layer of moist air in the lower troposphere. The two-channel algorithm involves three unknowns: surface temperature, air temperature, and integrated water vapor. Consequently, the calculation requires one empirical parameter derived from conventional weather data. We use the "average brightness temperature" for the lower troposphere, determined at clear radiosonde sites imbedded within the VAS radiance field. The algorithm is refined on simulated VAS data in order to

parameterize the average molecular absorption and to establish quality controls. Section 3 demonstrates the low-level moisture algorithm with one day of VAS data. A false color image sequence of precipitable water fields over the United States is computed from the split window radiances. The low-level water vapor patterns are also compared to the upper-level water vapor patterns inferred from the VAS 6.7 μm radiances. Areas are noted in which VAS indicates a strong vertical water vapor gradient before the outbreak of convective instabilities. The error budget for the split window algorithm is analysed, and the satellite-derived precipitable water estimates are verified by comparison to independent radiosonde reports. Section 4 summarizes the results and discusses possible extensions of the low-level moisture algorithm.

2.0 MODEL FOR LOW-LEVEL MOISTURE IN THE VAS SPLIT WINDOW

2.1 The VAS Split Window

A "split window" requires two channels at adjacent wavelengths in a fairly transparent region of the earth's atmospheric spectrum. Because the radiances in both channels are subject to nearly the same modifications by surface emissivity, aerosols and clouds, the difference in brightness temperature is controlled by the differential molecular absorption. The molecular and surface contributions to the radiance can be separated algebraically, and the molecular concentration can be determined from calculated values of the absorption cross sections. Naturally, the accuracy of this method depends upon several factors, including the accuracy of the radiometer, the field-of-view registration between the channels, the parameterization of molecular absorption cross sections, and the formulation of an algorithm which is robust enough to operate with only two channels and simple quality controls.

The VAS split window covers the 11 to 13 μm region of the earth's radiance spectrum, sketched in Figure 1. The window region is bracketed by the 10 μm ozone band and the 15 μm carbon dioxide band, with increasing molecular absorption at the longer wavelengths due to water vapor and carbon dioxide. The differential absorption was originally proposed as the basis for a correction to the sea surface temperature derived from the VISSR 11 μm window (Prahabekara, et al., 1974).

By contrast, our algorithm *removes* the background skin temperature in order to calculate the water vapor absorption in the lower troposphere.

The standard radiance weighting functions $d\tau/d\ln P$ are shown in Figure 2 for the VAS 11, 12 and 6.7 μm channels, and their shapes reflect the vertical water vapor profile of the U.S. Standard Atmosphere. The 11 and 12 μm channels transfer radiance from the entire lower troposphere (600 to 1000 mb), with the radiance exchange concentrated in the boundary layer, where most of the water content occurs. The other moisture-sensitive channel is centered on the strong 6.7 μm water vapor absorption band indicated in Figure 1. This bandpass has already been tested from polar orbit with NIMBUS-4 data (Rodgers, et al., 1976) and from geosynchronous orbit with METEOSAT data (Ramond, et al., 1981). The high-level 6.7 μm water vapor patterns can be compared to the low-level 11 and 12 μm water vapor patterns in order to infer the vertical water vapor structure (Petersen, et al., 1982).

2.2 The Single-Layer Model

A single-layer radiation model for the low-level water vapor is suited to the limited vertical resolution of the VAS 11 and 12 μm channels shown in Figure 2. The main features of the model are: a surface radiating at an effective temperature T_s, a layer of air radiating at an average temperature T_a, and a satellite-observed brightness temperature of T^*_ν in channel ν. The water vapor-determined transmissivity τ_ν controls the blend of surface and air brightness in a linearized radiation transfer equation:

$$\begin{aligned} T^*_\nu &= T_s\,\tau_\nu + T_a\,(1-\tau_\nu), \\ \tau_\nu &= (T^*_\nu - T_a)/(T_s - T_a). \end{aligned} \qquad (1)$$

In the first form of (1), surface radiance is attenuated by the factor τ and is replaced by the corresponding fraction $1-\tau$ from the air. The net effect is controlled by both the surface-to-air temperature contrast and the available water vapor. For example, $T_a = 280°K$ air attenuating the view of a $T_s = 300°K$ surface produces a $T^* = 292°K$ scene when $\tau = 0.60$. Previous VAS studies

(Chesters, et al., 1981 and 1982) attempted to use the simple algebraic difference between the split window brightness temperatures, $T^*_{12} - T^*_{11}$, as a measure of the water vapor content. However, both theory and practice show that a considerable fraction of the underlying surface temperature confuses this water vapor indicator.

In the second form of (1), the transmissivity is expressed as the fraction of the surface-to-air temperature contrast which is visible from the satellite. The transmissivity ratio between the 11 and 12 μm split window then removes the surface temperature algebraically:

$$\tau_{12}/\tau_{11} = (T^*_{12} - T_a)/(T^*_{11} - T_a). \tag{2}$$

The steps required for the application of (2) to the VAS split window are: (a) a simple parameterization linking the transmissivity ratio to the water vapor content, and (b) an empirical method for determining the average air temperature.

2.3 Parameterizing the Transmissivity

Transmissivity $\tau(\nu, P)$ is the probability of the satellite observing a photon at wavenumber ν after it has passed up through the atmosphere from pressure level P. The total transmissivity can be computed exactly from radiosonde temperature T(P) and water vapor Q(P) profiles as the product of the dry transmissivity through the well mixed gases (CO_2, NO, CH_4, N_2 and O_2) times the wet transmissivity over the water vapor profile:

$$\tau^{tot} = \tau^{dry}\,\tau^{wet},$$

$$\tau(\nu, P) = \exp(-k(\nu, P)\sec(\theta)), \tag{3}$$

$$k(\nu, P) = \int_P^{space} Q(P')\,da(\nu, P', T(P')).$$

Exact transmissivity calculations like (3) must be done laboriously from molecular line-by-line cross sections (McClatchey, et al., 1973) and p-type and e-type continuum cross sections (Roberts, et al., 1976), whose sum provides the absorption cross section $da(\nu, P', T(P'))$ at pressure P'. The absorption coefficient $k(\nu, P)$ is the vertical integral over the product of the temperature-sensitive

cross section $da(\nu, P', T(P'))$ and the molecular concentration profile $Q(P')$. The absorption along a line of sight is proportional to the projection factor $\sec(\theta)$, where θ is the zenith angle from a field-of-view to the satellite through a plane parallel atmosphere. Minor effects due to ozone absorption, the carbon dioxide continuum, and aerosol scattering are neglected in our calculations.

For the VAS bands, the water vapor absorption cross section is approximately twice as great at 12 μm as at 11 μm. The transmissivity in the VAS 11 μm channel is typically $\tau_{11} = 0.60$. Consequently, the satellite receives roughly 60% of the photons emitted by the surface at 11 μm, and only 36% (i.e., 0.60^2) at 12 μm. For practical use in real-time computations, the transmissivity at every VAS field-of-view is estimated from average values of the wet and dry absorption for the single layer atmospheric model.

The water vapor absorption at 11 and 12 μm is parameterized as the product of an average absorption cross section a^{wet} and the precipitable water PW (measured in gm cm^{-2}) projected on the line-of-sight:

$$\begin{aligned} \tau^{wet} &= \exp(-k^{wet} \sec(\theta)), \\ k^{wet} &= a^{wet} PW, \\ PW &= g^{-1} \int_{surface}^{space} Q(P)\, dP. \end{aligned} \tag{4}$$

The absorption coefficient for the well mixed gases k^{dry} is parameterized with a linear term to account for the modest effect of air temperature upon the CO_2 absorption:

$$\begin{aligned} \tau^{dry} &= \exp(-k^{dry} \sec(\theta)), \\ k^{dry} &= k + (dk/dT)(T_a - 280). \end{aligned} \tag{5}$$

The average wet and dry absorption parameters (a^{wet}, k and dk/dT) in (4) and (5) are determined by least squares fits to exact multi-layer transmissivity calculations for a wide ranging (arctic to tropical) set of 32 radiosonde reports, simulated at zenith angles from 0° to 60°. The average values are listed in Table 1 for the VAS 11 and 12 μm channels. They should apply with acceptable

Table 1.
Wet and dry absorption parameters for the lower troposphere, derived from least squares fits to wide ranging simulations of transmissivity for the VAS split window channels at 11 and 12 μm.

Channel	ν (cm^{-1})	a^{wet} (gm^{-1} cm^2)	k	dk/dT (K^{-1})
12 μm	789.24	0.3169	0.06114	0.00091
11 μm	897.40	0.1591	0.01066	0.00019

precision to any clear VAS field-of-view. The RMS error over the global range of simulated conditions was ±0.035 in the transmissivity ratio τ_{12}/τ_{11}. The error in this ratio for the 13 July 1981 VAS data is approximately ±0.025, corresponding to only ±0.3 gm cm^{-2} uncertainty in a moisture burden of 5.0 gm cm^{-2} along the line-of-sight. Consequently, errors due to the transmissivity parameterization will contribute less than 10% uncertainty to the satellite-derived water burden.

2.4 The Average Air Brightness Temperature

Finally, precipitable water is related to the brightness temperatures and average air temperature by combining (2), (4) and (5) and the information in Table 1 into the following set of equations:

$$PW = \frac{-\ln (\tau_{12}{}^{wet} / \tau_{11}{}^{wet})}{(a_{12}{}^{wet} - a_{11}{}^{wet}) \sec(\theta)} ,$$

$$\tau_{12}{}^{wet} / \tau_{11}{}^{wet} = \frac{(T^*_{12} - T_a) / (T^*_{11} - T_a)}{\exp(-\Delta k^{dry} \sec(\theta))} , \qquad (6)$$

$$\Delta k^{dry} = (k_{12} - k_{11}) + (dk_{12}/dT - dk_{11}/dT)(T_a - 280K).$$

Given the satellite observed brightnesses, T^*_{12} and T^*_{11}, one can first use (6) to estimate T_a from PW values at some radiosonde sites imbedded within the radiance field. Then, one can use this

average radiosonde-based value of T_a to make satellite estimates of PW over the rest of the field. The model represented by (6) actually treats the "average air temperature" T_a as an empirical parameter which accounts for the lower tropospheric radiance. An even simpler empirical method for determining T_a is to adjust it by hand until the satellite-derived precipitable water values nearly match the values expected within the scene. This human interactive method is especially useful when the scene's precipitable water content can only be estimated from climatological considerations, such as for oceanic fields. Of course, more elaborate horizontal models for T_a could be devised, such as gradients, air masses or objective analyses between sites.

The sensitivity of satellite-derived precipitable water to the air temperature can be estimated from (6) as the derivative dPW/dT_a. For typical mid-summer conditions of $T_s = 300$ K, $T_a = 280$ K, $PW = 4$ gm cm^{-2} and $\sec(\theta) = 1.25$, the sensitivity is $dPW/dT_a = 0.6$ gm cm^{-2} K^{-1}. The sensitivity to radiometric errors is a comparable value. Such sensitivity is undoubtedly related to the substantial absolute errors which were found in previous studies of satellite-derived water vapor fields. Like those studies, this report finds evidence for very good determination of water vapor gradients, but less certain absolute accuracy. Indeed the average air temperature T_a in (6) acts like a water vapor scaling parameter, and the empirical approach to its determination at ground truth sites is intended to cancel as many biases as possible.

3.0 VAS SPLIT WINDOW OBSERVATIONS OF LOW-LEVEL WATER VAPOR

3.1 Case Study, 13 July 1981

At 1200 GMT on 13 July 1981, a weak surface low was drifting slowly from eastern Colorado toward Nebraska, with a cold front extending from Nebraska toward northern Illinois and into the southern Great Lakes region (Figure 3-A). The southeastern United States was dominated by a broad high pressure system centered near the Mississippi-Alabama border. The resultant anticyclonic circulation forced a southerly air flow over a rather broad band west of the Mississippi River. This air was noticeably and uniformly humid with surface dewpoints greater than 20°C over the region from the Gulf of Mexico northward into southern Minnesota, and with dewpoints greater

than 24°C located both in southern Illinois and near the Gulf Coast. Precipitation observed by radar (Figure 3-D) was mainly confined to thunderstorms along and to the north of the cold front, extending along a line from South Dakota to the Ohio valley. Weak thunderstorms and showers were also reported in the Texas-Louisiana coastal area.

By 1800 GMT, the southerly air flow and the morning insolation had forced surface temperatures to rise well above 30°C over the central United States, while the dewpoints remained high (Figure 3-B). Two distinct dewpoint maxima are observed, one directed from the Gulf of Mexico toward eastern Oklahoma and the other extending from Iowa to Ohio. A noticeable gradient in the dewpoints is evident in the area between eastern Colorado and eastern Kansas. The thunderstorms originally in South Dakota had drifted northward and diminished in intensity, while the storms originally in Iowa had weakened considerably as they moved into Illinois (Figure 3-E). The convection along the Gulf Coast continued to intensify, and numerous rain and thundershowers were reported east of the Mississippi River.

By 0000 GMT on 14 July 1981, the surface dewpoints exceeded 24°C in two regions: in the Gulf States region extending northward to eastern Oklahoma, and immediately ahead of the now warm front in Iowa and west central Illinois (Figure 3-C). The dewpoint gradient from eastern Nebraska to Kansas strengthened considerably as drier air moved east-northeast from Colorado into Nebraska. Scattered rainshowers had developed in the area of Kansas, Oklahoma and Arkansas, and heavier thunderstorms developed from New Mexico to western Nebraska, while the band of thunderstorms continued along the Texas-Gulf Coast region (Figure 3-F). In Iowa, intense thunderstorms with tops approaching 18,000 m developed south of the frontal zone and were accompanied by weaker cells in extreme eastern Nebraska.

Our application of the VAS split window will focus upon the changes in the water vapor field in the middle portion of the United States, where (a) convection persisted along the Gulf Coast, (b) scattered rain showers developed in Oklahoma, and (c) intense thunderstorms went through various stages of development in Iowa and Illinois.

3.2 Satellite Imagery and Quality Control

Satellite images also help to set the scene for application of the low-level water vapor algorithm. Figure 4 contains four satellite images of the United States at mid-morning on 13 July 1981:

a. Figure 4-A is an operational visible VISSR image taken from SMS-3 at 1430 GMT. At 1 km resolution, it shows that the central United States is relatively cloud free, demonstrating that unresolved clouds are not a serious hazard at this time to processing the VAS thermal infrared data at 15 km resolution. Visible imagery is not available at 1200 GMT, due to the low sun angle at that time, so that we must assume similar cloud conditions during the preceeding VAS and radiosonde observations. Visible imagery taken after 1500 GMT shows the development of broken clouds over much of the east-central United States, along with the development of overcast conditions in the regions of precipitation found in Figures 3-E and 3-F.

b. Figure 4-B is the VAS 11 μm infrared image taken from GOES-5 at 1500 GMT. For inter-channel comparisons, the radiances have been converted to brightness temperature over a range from 200° to 320°K, with a false color spectrum assigned in 10°K steps. Each color is shaded internally to display detailed gradients more clearly. A typical clear pixel in the central United States has T^*_{11} between 290° and 300°K, with false color red. One can see a 10°K gradient between the high plains and the central river valleys, but still little contrast between the land and water areas. By 2100 GMT, the VAS 11 μm images of the central United States brightened by another 10°K, while the clear oceanic areas remained about the same. This is a substantial dynamic range of underlying surface temperatures to remove from the split window water vapor estimates. The cloudy areas in Figure 4-B are radiometrically colder, from 220° to 280°K, and are colored with yellows, greens, blues and whites. Radiosonde sites which were judged to be cloud free at 1200 GMT are indicated with their station names on this 1500 GMT image.

c. Figure 4–C is the corresponding VAS 12 μm image at 1500 GMT. Since the water vapor attenuation is greater at 12 μm, the brightness temperatures are 5° to 10°K less than found in the 11 μm window. The central plains show T^*_{12} between 280° and 290°K, shifted by almost one 10°K false color step (from red to orange) with respect to Figure 4–B, while the unattenuated cloud top temperatures remain the same.

d. Figure 4–D is the corresponding VAS 6.7 μm brightness temperature image at 1500 GMT. As expected from the radiance weighting function in Figure 2, this channel appears much colder than the window channels. The surface features are totally hidden by the upper-tropospheric water vapor, and only the tops of the higher clouds appear as "landmarks" which can be found in the other panels of Figure 4. Subsynoptic upper-level water vapor patterns appear as cold, relatively wet areas (colored dark green, near 240°K) mixed with warm, relatively dry areas (colored light green and yellow, near 250°K). The warmest streaks are interpreted as relatively transparent "dry slots" in the upper air, often associated with upper-level jets. A more detailed analysis of the upper-level water vapor patterns inferred from the VAS 6.7 μm channel has been reported separately for this case (Petersen, et al., 1982).

The 5 to 10°K difference between T^*_{11} and T^*_{12} in Figures 4–B and –C is used as the satellite "signal" for precipitable water estimates.

The noise in the VAS split window channels is approximately ±0.5°K (Chesters, et al., 1981). Since the split window brightness temperature difference is 5° to 10°K, the signal/noise ratio is approximately 10/1. Consequently, the water vapor estimates are noticeably limited by radiometric noise, even in clear air with a strong surface-to-air temperature contrast. When the T* difference is small or when either channel approaches T_a, the PW estimate from (6) becomes unreliable. Consequently, a series of simple threshold tests is used to identify doubtful fields-of-view:

$$\begin{aligned} &\text{Reject if } T^* - T_a < 1°K \text{ in either channel,} \\ &\quad \text{or } T^*_{12} - T^*_{11} < 1°K, \\ &\quad \text{or } PW > 10 \text{ gm cm}^{-2}. \end{aligned} \tag{7}$$

The air temperature threshold accounts for most of the rejected pixels, which are the cold cloud tops found in Figure 4. The two-channel threshold rejects pixels where the water vapor is covered by low clouds or fog. The precipitable water threshold is set rather high in order to provide some subjective quality control. Because PW greater than 6 gm cm^{-2} is physically unreasonable for our case, the excessive PW values indicate the location of clouds which are unresolved by the VAS 15 km footprint, warning the user to regard those areas with suspicion.

3.3 Empirical Air Temperature Estimate

The 1200 GMT lower troposphere's average air brightness temperature T_a was found by using radiosonde-derived PW values in (6) and (7) at the eleven clear fields-of-view indicated in Figure 4-B. The radiosonde-based air temperatures had no systematic variations within the 1200 GMT field, so that the average value (282.7 ± 1.3°K) was adopted. For this midsummer case, the average value of T_a was nearly equal to the average radiosonde temperature reported at 700 mb. Because T_a characterizes the mean brightness of the lower troposphere, its value should be little affected by diurnal heating of the boundary layer. Consequently, the value of T_a from the 1200 GMT radiosondes was extended to the VAS split window fields throughout the day, up to and including the subsequent radiosonde launch at 0000 GMT.

Of course, a single value for the air temperature cannot apply over an extremely large domain. For instance, the mean value of T_a from the central United States will produce both overestimates of the precipitable water in the distinctly colder air mass over the Great Lakes region and underestimates in the subtropics. The simple threshold tests in (7) will reject the substantially colder air mass in Canada (note the low 11 μm brightness temperatures in Figures 4-B and -C) and will even reject some of the cold waters in the Great Lakes themselves.

3.4 False Color Images of Low-Level Water Vapor

Figure 5 is a series of five false color images of the low-level water vapor derived from the VAS split window. The algorithm in (6) was applied to every pixel which was not rejected by the quality

controls in (7). The images were taken at three-hour intervals from 1200 GMT on 13 July 1981 to 0000 GMT on 14 July 1981. The PW range is from 0 to 10 gm cm^{-2}, with a change of hue on the false color spectrum every 1 gm cm^{-2}. Each hue is internally shaded to display detailed PW variations. Fields-of-view which were rejected by the quality control thresholds are colored black, and most of them obviously correspond to the cold cloud tops seen in Figure 4. Drier pixels are colored red, normal pixels are colored orange and yellow, wetter pixels are colored light green, and excessively wet pixels are colored dark green and blue.

For quality assurance, a histogram has been made of the precipitable water distribution of the processed pixels within each frame of Figure 5. The number of pixels with PW between 0 and 10 gm cm^{-2} is counted within 0.125 gm cm^{-2} bins. The pixels with PW greater than 6 gm cm^{-2} are probably contaminated by unresolved clouds. While they account for about 20% of the processed fields-of-view, they are clearly grouped into cloudlike patterns within the Gulf of Mexico and along the edges of the recognizable cloud masses. The histogram statistics remain nearly stationary over the 12-hour observing period, supporting the assumption that the average 1200 GMT air brightness temperature applies consistently throughout the day. There is a small shift toward lower average PW values by midday, which is consistent with a small actual increase in T_a due to daytime heating of the boundary layer at the bottom of the lower troposphere.

The low-level water vapor patterns in Figure 5 show vivid subsynoptic and mesoscale features at 15 km resolution evolving over the 12-hour observing period. The algorithm has eliminated all traces of the underlying 20°K range in skin temperatures observed in the 11 μm radiances during the day. The spatial and temporal continuity of the features is convincing qualitative evidence of the relative accuracy of the algorithm. For instance, the relatively cloud free area in the northwestern Gulf of Mexico serves as a "secondary standard" for the low-level water vapor, monitoring the temporal stability of the algorithm within a region of steady atmospheric and surface conditions. Likewise, the dry area in Nebraska monitors the temporal stability of the satellite-derived low-level water vapor within a region of steady atmospheric conditions but rapidly varying surface

temperature. A full spectrum of horizontal moisture variations is evident in Figure 5. Qualitatively, the amplitude of the variations is rather mild on the synoptic scale (due to the extension of a single value for the air temperature to the entire domain), quite large on the subsynoptic scale, moderate on the mesoscale, and again low on the local scale, with very little pixel-to-pixel variation which is not due to unresolved clouds.

On the subsynoptic scale, the VAS water vapor features in Figure 5 correspond to the general dewpoint patterns in the conventional surface analyses in Figure 3. For instance, the moist cloudy area in Arkansas drifts slowly into Oklahoma with the low-level flow, and develops convective elements by 2100 GMT. The surface dewpoint maximum in the Gulf States is somewhat masked by clouds in the satellite precipitable water images. Subsynoptic details include the intensifying arc of clouds and water vapor which propagates from the Gulf of Mexico into Texas. Likewise, the moisture gradient from Nebraska to Kansas (surface dewpoints from 10° to 20°C in Figure 3-A) is detected by the VAS split window (precipitable water from 2 to 5 gm cm^{-2} in Figure 5-A). This gradient strengthens in both analyses over the 12-hour observing period, as a markedly dry feature moves northeastward across Nebraska, growing to the south of a developing low pressure area. In fact, all of the VAS-derived subsynoptic moisture features over the central United States are confirmed at the lower resolution of the conventional analyses. The regional moisture features which are normally unobserved in the conventionally data-void areas, such as the Gulf of Mexico and the Atlantic Ocean, are subjectively verified by the continuity of their development.

On the mesoscale, the VAS split window images in Figure 5 display vivid structures and significant changes within the subsynoptic features. For instance, the satellite-derived water vapor images depict the evolution of the broad moisture maximum in Arkansas and Kansas into two separate moisture bands within which convective clouds ultimately develop. By 0000 GMT, the precipitation pattern in the Oklahoma region (Figure 3-F) reflects the distinct low-level moisture pattern (Figure 5-E). Likewise, Iowa was the scene of interesting changes during the 12-hour period. After the morning thunderstorms dissipate over eastern Iowa, a water vapor maximum remains at 2100 GMT (Figure 5-D). By 0000 GMT, new thunderstorms develop in southern and

eastern Iowa, within a local water vapor maximum and along a water vapor gradient, respectively (see Figures 3-F and 5-E). The storms along the water vapor gradient in southern Iowa are located 150 km behind the warm frontal zone, which remains in northern Iowa during this period (Figure 3-C). Another interesting example of mesoscale variability is found within the stable dry feature in Nebraska. The single dry zone originally in southwest Nebraska slowly propagates northeastward between 1500 and 1800 GMT and then is rapidly enlarged by the development of a second dry zone in northeastern Nebraska between 2100 and 0000 GMT (Figures 5-C, -D and -E). Thus, the increase in the conventional surface dewpoint gradient across eastern Nebraska (Figures 3-B and -C) appears to be the result not only of the advection of the original dry air but also the rapid formation of a second dry region, perhaps due to the downward transport of mid-tropospheric air.

Figure 5 reveals a wealth of high-resolution details and rapid changes within the VAS-derived low-level moisture fields which cannot be fully confirmed by the conventional radiosonde or surface networks. The changing mesoscale moisture fields in the Iowa region provide an excellent example of the limitations of using conventional analyses for verification of satellite data. There are no radiosonde stations in the entire state of Iowa to corroborate the VAS-observed precipitable water in the lower troposphere, and the hourly surface data lacks the vertical information necessary to verify integrated water vapor content. In particular, the conventional surface stations within Iowa and central Illinois report dewpoints approaching 24°C in a band extending immediately south of the warm front (Figure 3-C), where the satellite measurements of precipitable water are also large. However, the surface dewpoints are relatively uniform throughout Iowa, Illinois and Missouri, while the VAS precipitable water field (Figure 5-D) exhibits a narrow band of significantly drier air which extends from central Nebraska through northern Missouri, and into Illinois. Therefore, the VAS split window apparently can differentiate between those areas in which the water vapor extends over a deep layer (more able to supply convective cells) and those areas in which the water vapor is confined to a rather shallow boundary layer (less able to support convection). Another example of the mesoscale limitations of conventional analyses is revealed by comparing the smooth

surface dewpoint gradient extending from Nebraska to Oklahoma with the complex VAS moisture patterns in the same region. The VAS integrated water vapor images show a separate band of moisture and showers from north Texas to central Kansas at 0000 GMT (Figure 5-E) which is located *to the west* of the dewpoint gradient analyzed from the surface data (Figure 3-C). Apparently, moist air from the east is overrunning a shallow dry layer which still envelops the surface-level stations. Once again, convective clouds and rain developed within a VAS-determined water vapor maximum, as they did in Iowa.

In summary, the sequence of low-level water vapor fields in Figure 5 demonstrates that the VAS instrument meets its objectives of monitoring rapid mesoscale variations from geosynchronous station and of filling the space-time gaps in the conventional regional coverage.

3.5 Contrast to High-Level Water Vapor

The radiance weighting functions in Figure 2 indicate that the low-level water vapor patterns from the 11 and 12 μm channels are radiometrically independent of the high-level patterns observed in the 6.7 μm channel, so that a correlation between the two images reflects an actual physical correlation in the vertical water vapor structure. For example, the 1500 GMT images in Figures 5-B and 4-D show similar patterns in the moisture structure over the Great Lakes region, but different patterns in the moisture structure over the central Great Plains. In fact, the 0000 GMT thunderstorms in Iowa were preceeded by the advection of dry air (inferred from the 6.7 μm channel) over the low-level moisture concentration (computed from the VAS split window). A detailed comparison of the entire series of low- and high-level water vapor images is the subject of a separate paper (Petersen, et al., 1982).

3.6 Quantitative Verification and Error Analysis

For quantitative verification of the satellite-derived, low-level water vapor values, the conventional radiosonde network is the only available source of "ground truth" data. The 1200 GMT reports on 13 July 1981 were used to establish the average air temperature, so they do not provide a

completely independent measure of the error. At that time, from the appearance of the VAS images, from radiometric quality controls, and from the stations' own reports of cloud cover, eleven sites were judged to be cloud free. The open circles in Figure 6 compare the satellite-derived precipitable water to the radiosonde-derived values, showing an RMS difference of ±0.88 gm cm^{-2}. The errors are dominated by a disagreement of 1.94 gm cm^{-2} at International Falls, Minnesota, which is located within a different air mass from most of the other training sites in the central United States.

The 0000 GMT 14 July 1981 radiosonde reports provide a completely *independent* quantitative measure of the accuracy, twelve hours after the determination of the air temperature. At this later time, twenty-four sites were accepted by the algorithm's threshold tests. The filled circles in Figure 6 compare the satellite-derived precipitable water to the radiosonde values. The correlation coefficient of the independent set is 0.78, with an RMS error of ±0.67 gm cm^{-2} over a range of 1.8 to 5.3 gm cm^{-2}. The mean error for the 0000 GMT verification sites was -0.28 gm cm^{-2}, which could be explained by an actual increase in the average air temperature by +0.4°K during the twelve daylight hours following the 1200 GMT determination of T_a. The worst error in the verification is associated with Sault Sainte Marie, Michigan, which reported overcast conditions at 0000 GMT and which is located in a different air mass from the 1200 GMT training area in the United States. Some of the other test sites were also reporting scattered or broken clouds at 0000 GMT. Obviously, the threshold tests on the split window do not remove all cloud contamination from the water vapor estimate.

The *quantitative* verification of the satellite-derived precipitable water at "ground truth" sites indicates fairly good absolute accuracy over a large range of water vapor content. The *qualitative* verification provided by the spatial and temporal continuity of the low-level water vapor fields indicates very good relative accuracy at high horizontal resolution. The error budget is dominated by radiometric noise, clouds and model limitations:

a. The VAS radiometric errors are approximately ±0.5°K compared to a typical 5.0°K contrast in the split window brightness temperatures. The radiometric noise contributes about ±0.4 gm cm^{-2} to the error budget for this case.

b. Unresolved clouds cause systematic errors which are more difficult to quantify. Simulations with cloud cover terms in (1) indicate that clouds colder than the average air temperature cause precipitable water overestimates in (6), and warm clouds or fog cause underestimates. Unfortunately, the use of more severe thresholds for the split window would suppress genuine subsynoptic features in the colder areas, such as the Great Lakes region.

c. The errors due to simplifications by the linearized single layer model for the lower troposphere are also difficult to quantify. From simulations, the random errors in the absorption coefficient parameterization are estimated to contribute approximately ±0.3 gm cm^{-2}. The systematic errors from using a simple average air temperature are scarcely detectable (less than 0.3 gm cm^{-2}) in the statistical, horizontal and temporal behavior of the precipitable water fields in Figure 5. Unfortunately, a more complicated model would introduce more unknowns to be determined. The use of more VAS channels would likewise introduce more unknowns, by sacrificing the split window's cancellation of several variables in the field-of-view, such as surface emissivity.

Altogether, the random radiometric and parametric errors contribute approximately ±0.5 gm cm^{-2} uncertainty to the precipitable water estimate, accounting for one-half of the variance in the observed ±0.7 gm cm^{-2} RMS error. The remaining variance is due to more systematic errors from unresolved clouds, model limitations and air temperature variations.

In summary, the quantitative and qualitative verification of low-level water vapor from the VAS split window shows fairly good absolute and very good relative accuracy, respectively. The algorithm is robust enough to extract precipitable water information from just two VAS window

channels. The background surface temperature variations are eliminated quite effectively, and the residual errors are dominated by noise and unresolved clouds.

4.0 SUMMARY AND DISCUSSION

Fields of low-level atmospheric water vapor are derived from the "split window" 11 and 12 μm infrared channels of the VISSR Atmospheric Sounder (VAS) carried on the GOES-5 satellite. The differential water vapor absorption between the two channels allows the separation of surface and atmospheric radiances within a field-of-view. The average air brightness temperature, determined at radiosonde sites, allows the further separation of atmospheric emission and absorption terms. A simply parameterized algorithm is developed from a single-layer model for the split window radiances. The vertically integrated water vapor content (measured in gm cm^{-2}) of the lower troposphere is then estimated from a time-sequence of five VAS split window images taken every 3 hours over the United States on 13 July 1981. False color images of the integrated water vapor show vivid subsynoptic and mesoscale details at 15 km horizontal resolution which evolve continuously during the 12-hour period. Precipitable water estimates are verified with independent radiosonde measurements taken 12 hours after the initial air temperature determination, and an accuracy of ±0.67 gm cm^{-2} is established over a range of 1.8 to 5.3 gm cm^{-2}. Cloudy fields-of-view are detected as being colder than the air, and are simply rejected from the images. Unresolved clouds are readily identified as cloudlike patterns of excessive water vapor in the images. Several areas of enhanced low-level water vapor develop into convective cloud formations. Convective cloud formation is most vigorous in an area of initially clear air with a strong vertical water vapor gradient (where the upper-level water vapor content is inferred directly from the VAS 6.7 μm radiances). The sequence of low-level water vapor fields in Figure 5 demonstrates that the VAS instrument meets its objectives of monitoring rapid mesoscale variations from geosynchronous station and of filling the space-time gaps in the conventional regional coverage.

This midsummer day of VAS data provides a wealth of detail for satellite retrieval and mesoscale development studies. Vertical water vapor structure has already been inferred by comparing

the 6.7 μm channel to the low-level moisture fields derived from the split window, and a preliminary meteorological analysis has been made from mesoscale fields of VAS multi-channel soundings (Petersen, et al., 1982). The split window estimates are currently being compared to water vapor profile retrievals derived from all the VAS channels and other conventional data, and a detailed meteorological analysis is being made of the VAS-derived mesoscale developments associated with the Iowa thunderstorms.

The split window, low-level moisture algorithm itself will be tested and extended with more case studies. For instance, the two window channels will be supplemented with the VAS low-level temperature sounding channels in order to provide a direct estimate for the "air brightness temperature" at each field-of-view, instead of using an empirical average from imbedded radiosonde sites. Likewise, the other infrared channels can provide better quality control over the cloud-contaminated fields-of-view. In addition, collocated visible data is available at 1 km resolution in the VAS data stream which could be used to detect clouds that are not resolved with the 15 km thermal detectors. The data-void oceans might be processed more accurately with a rearrangement of the algorithm to use the sea surface temperature instead of the average air temperature as ancillary conventional data. The algorithm will probably be less effective in the drier winter air over the United States, in the cloud- and water vapor-obscured tropics, and in any situation where the surface-to-air temperature contrast is small. Although automatic processing of two VAS channels is not as accurate as human interactive, multi-channel retrievals followed by an objective analysis, the real-time image sequences can draw a user's attention to otherwise undetected mesoscale water vapor features within relatively clear air. Ultimately, the utility of the VAS-derived water vapor patterns will be judged by their acceptance as a mesoscale nowcasting and forecasting tool, when the VAS moisture channels are distributed as a product of the operational GOES system.

ACKNOWLEDGMENTS

This work is funded through the VAS Demonstration Project of NASA's Operational Satellite Improvement Program (OSIP), and is managed by Mr. James Greaves of NASA/GSFC. Dr. Harry

Montgomery of NASA/GSFC coordinated the data collection during the post-launch testing and demonstration period in the summer of 1981. We thank Mr. Anthony Mostek of Computer Sciences Corporation for preparing some datasets for our use and for reviewing this manuscript.

REFERENCES

Chesters D., L. W. Uccellini, H. Montgomery, A. Mostek and W. Robinson, 1981: *Assessment of the first radiances received from the VISSR Atmospheric Sounder (VAS) Instrument*, NASA TM 83827. (Available as NTIS-81NO12678).

Chesters D., L. W. Uccellini and A. Mostek, 1982: "VISSR Atmospheric Sounder (VAS) Simulation Experiment for a Severe Storm Environment," *Mon. Wea. Rev., 110,* 198-216.

Hillger D. W. and T. H. Vonder Haar, 1981: "Retrieval and use of high-resolution moisture and stability fields from NIMBUS-6 HIRS radiances in pre-convective situations," *Mon. Wea. Rev., 109,* 1778-1806.

McClatchey R. A., W. S. Benedict, S. A. Clough, D. E. Burch, R. F. Calfee, K. Fox, L. S. Rothman and J. S. Garing, 1973: *AFCRL atmospheric absorption line parameter compilation*, AFCRL-73-0096. (Available as NTIS-73N30382).

Menzel W. P., W. L. Smith and L. D. Herman, 1981: "Visible infrared spin-scan radiometer atmospheric sounder radiometric calibration: an inflight evaluation from intercomparisons with HIRS and radiosonde measurements," *Applied Optics, 20,* 3641-3644.

Petersen R. A., L. W. Uccellini, D. Chesters, D. Keyser and A. Mostek, 1982: "The use of VAS satellite data in weather analysis, prediction and diagnosis," *Ninth Conf. for Weather Forecasting and Analysis*, Seattle, Washington. Published by the Amer. Meteor. Society.

Phillips N., L. M. McMillan, A. Gruber and D. W. Wark, '979: "An evaluation of early operational temperature soundings from TIROS-N," *Bull. Amer. Meteor. Soc., 16,* 1188-1197.

Prahabakara C., G. Dalu and V. G. Kunde, 1974: "Estimation of sea surface temperature from remote sensing in the 11 to 13 micron window region," *J. Geophys. Res., 79,* 5039-5044.

Ramond D., H. Corbin, M. Desbois, G. Szejwach and P. Waldteufel, 1981: "The dynamics of polar jet streams as depicted by the METEOSAT water vapor channel radiance field," *Mon. Wea. Rev., 109,* 2164–2176.

Roberts R. E., J. E. A. Selby and L. M. Biberman, 1976: "Infrared continuum absorption by atmospheric water vapor in the 8–12 micron window," *Applied Optics, 15,* 2085–2090.

Rodgers E. B., V. V. Salmonson and H. L. Kyle, 1976: "Upper tropospheric dynamics as reflected in NIMBUS–4 THIR 6.7 μm data," *J. Geophys. Res., 81,* 5749–5758.

Schlatter T. W., 1981: "An assessment of operational TIROS–N temperature retrievals over the United States," *Mon. Wea. Rev., 109,* 110–119.

Smith, W. L., V. E. Suomi, W. P. Menzel, H. M. Woolf, L. A. Sromovsky, H. E. Revercomb, C. M. Hayden, D. N. Dickson and F. R. Mosher, 1981: "First sounding results from VAS–D," *Bull. Amer. Meteor. Soc., 62,* 230–236.

Suomi V. E., T. Vonder Haar, R. Kraus and A. Stamm, 1971: "Possibilities for sounding the atmosphere from a geosynchronous spacecraft," *Space Research XI,* 609–617.

FIGURE CAPTIONS

Figure 1: The VAS water vapor channels illustrated by (A) a sketch of the earth's radiance spectrum compared to (B) the filter response functions at 11, 12 and 6.7 μm.

Figure 2: Radiance weighting functions for the VAS water vapor channels at 11, 12 and 6.7 μm.

Figure 3: NWS maps of conventional surface data shown at: (A) 1200 GMT on 13 July 1981, (B) 1800 GMT on 13 July 1981 and (C) 0000 GMT on 14 July 1981; the solid lines are isobars (e.g. 16 = 1016 mb) and the dashed lines are isodrosotherms (°C). The corresponding radar precipitation maps are shown at : (D) 1135 GMT, (E) 1735 GMT and (F) 2335 GMT on 13 July 1981; maximum tops (dkm) are underlined, and an arrow with a number indicates direction and speed (m s^{-1}) for the convective system.

Figure 4: Midmorning satellite images of the United States on 13 July 1981: (A) the VISSR visible image from SMS-3 at 1430 GMT, (B) the VAS 11 μm image from GOES-5 at 1500 GMT (color coded as brightness temperature from 200 to 320 K, and marked with radiosonde sites which were cloud free at 1200 GMT), (C) the corresponding VAS 12 μm channel and (D) the corresponding VAS 6.7 μm channel.

Figure 5: Image sequence of five low-level water vapor estimates from the VAS split window over the United States, made at 3-hour intervals starting from 1200 GMT on 13 July 1981. The images are encoded with a false color spectrum for precipitable water values from 0 to 10 gm cm^{-2}. Pixels below the assumed air temperature are assumed to be cold cloud tops and are colored black. A histogram of the number of pixels with satellite-derived PW values is displayed beneath each image, with a distribution that remains nearly constant throughout the day.

Figure 6: Plot of radiosonde-derived "ground truth" precipitable water values compared with the corresponding VAS-derived values: (o) 11 clear radiosonde sites at 1200 GMT on 13 July 1981, used to determine T_a for the scene throughout the day, and (●) 24 independent radiosonde sites at 0000 GMT on 14 July 1981.

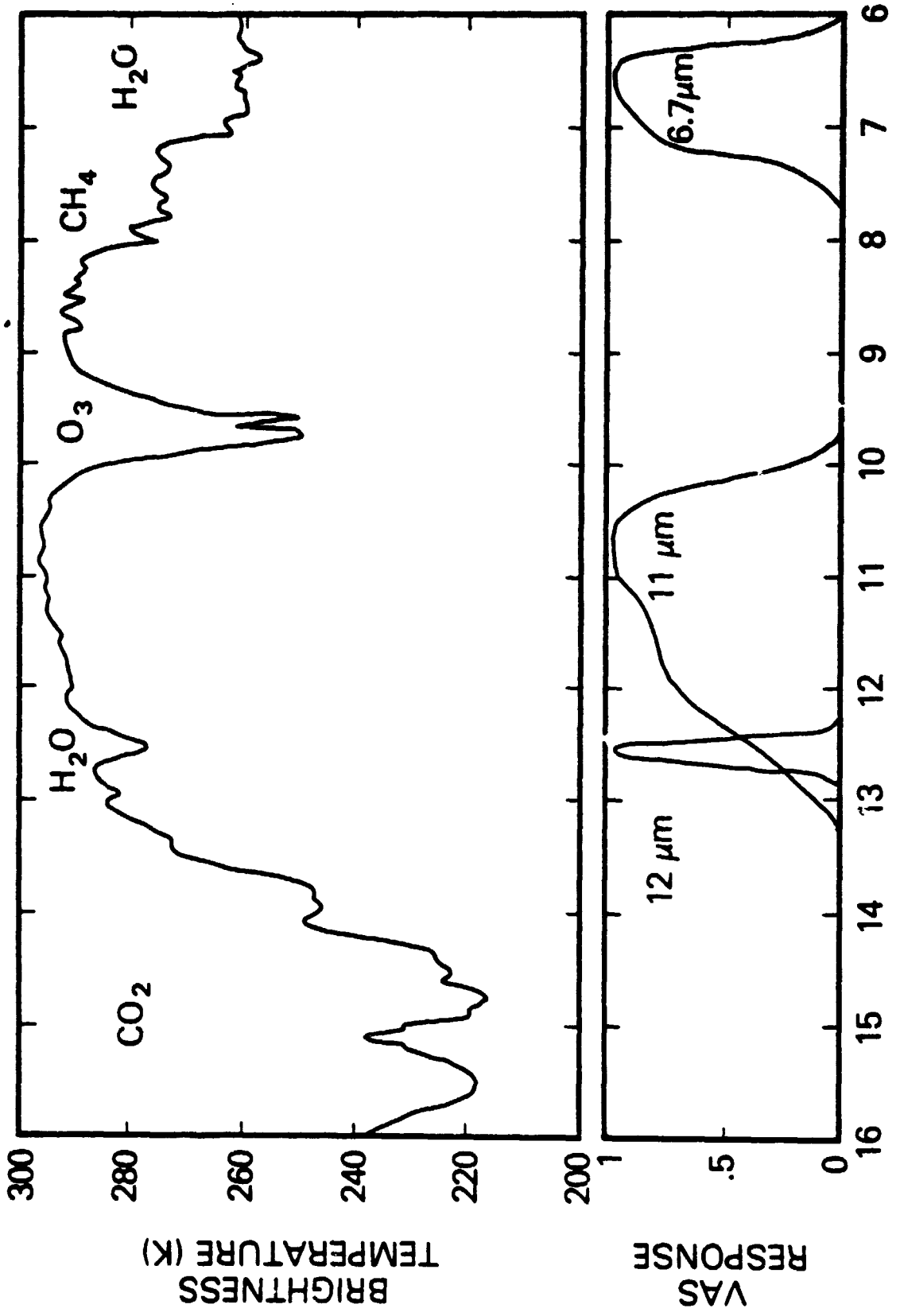

Figure 1.

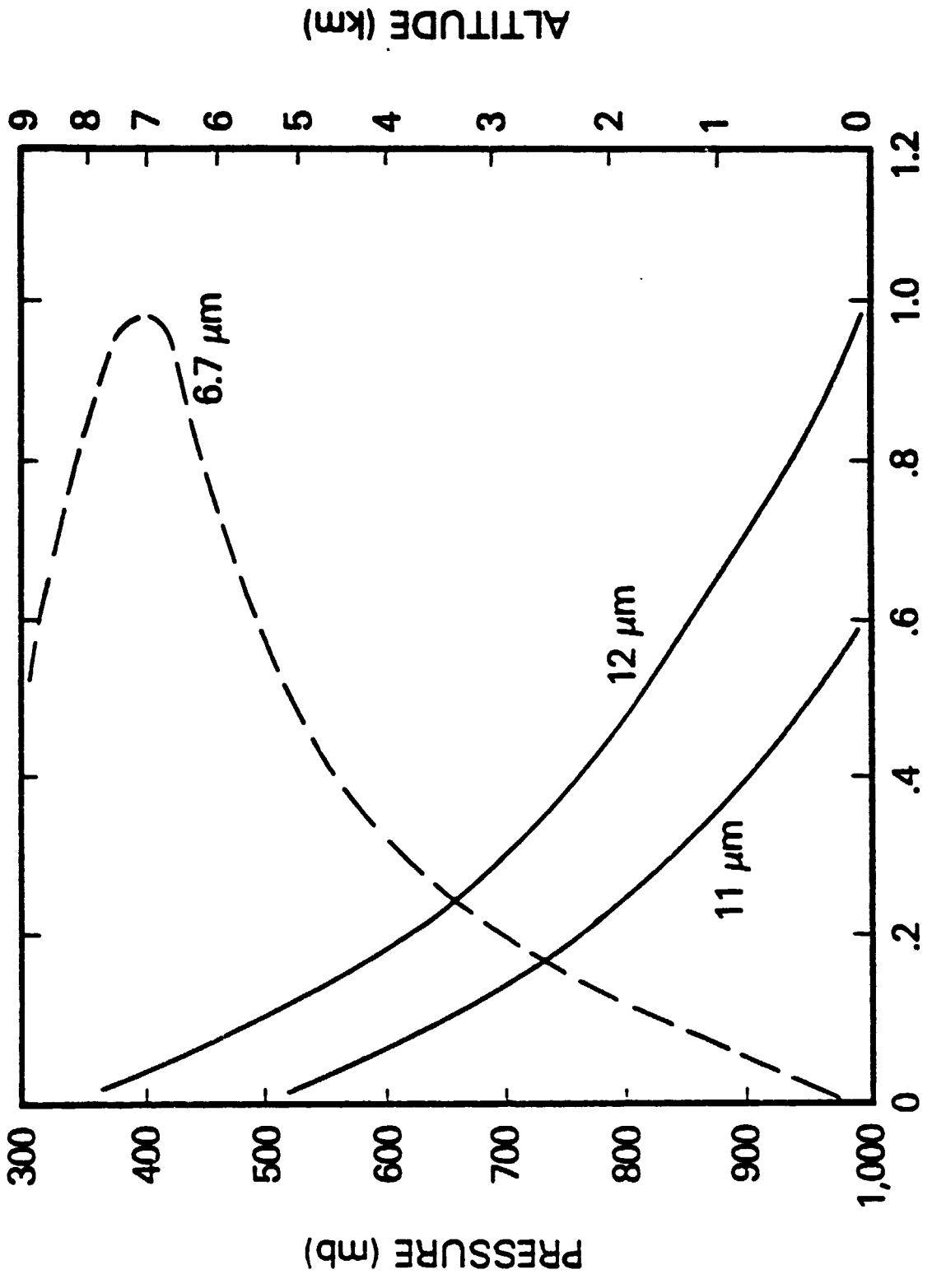

Figure 2.

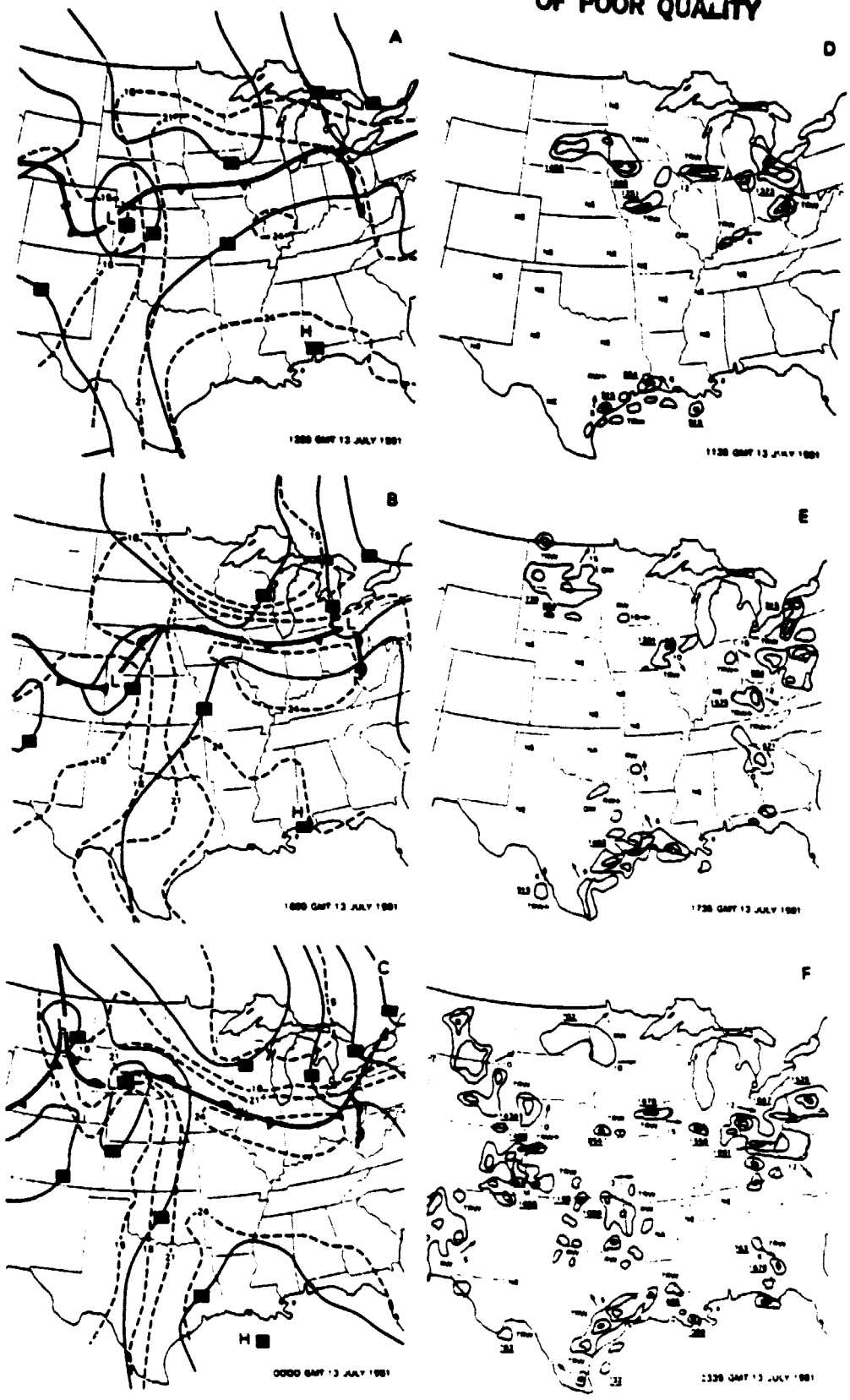

Figure 3.

ORIGINAL PAGE
COLOR PHOTOGRAPH

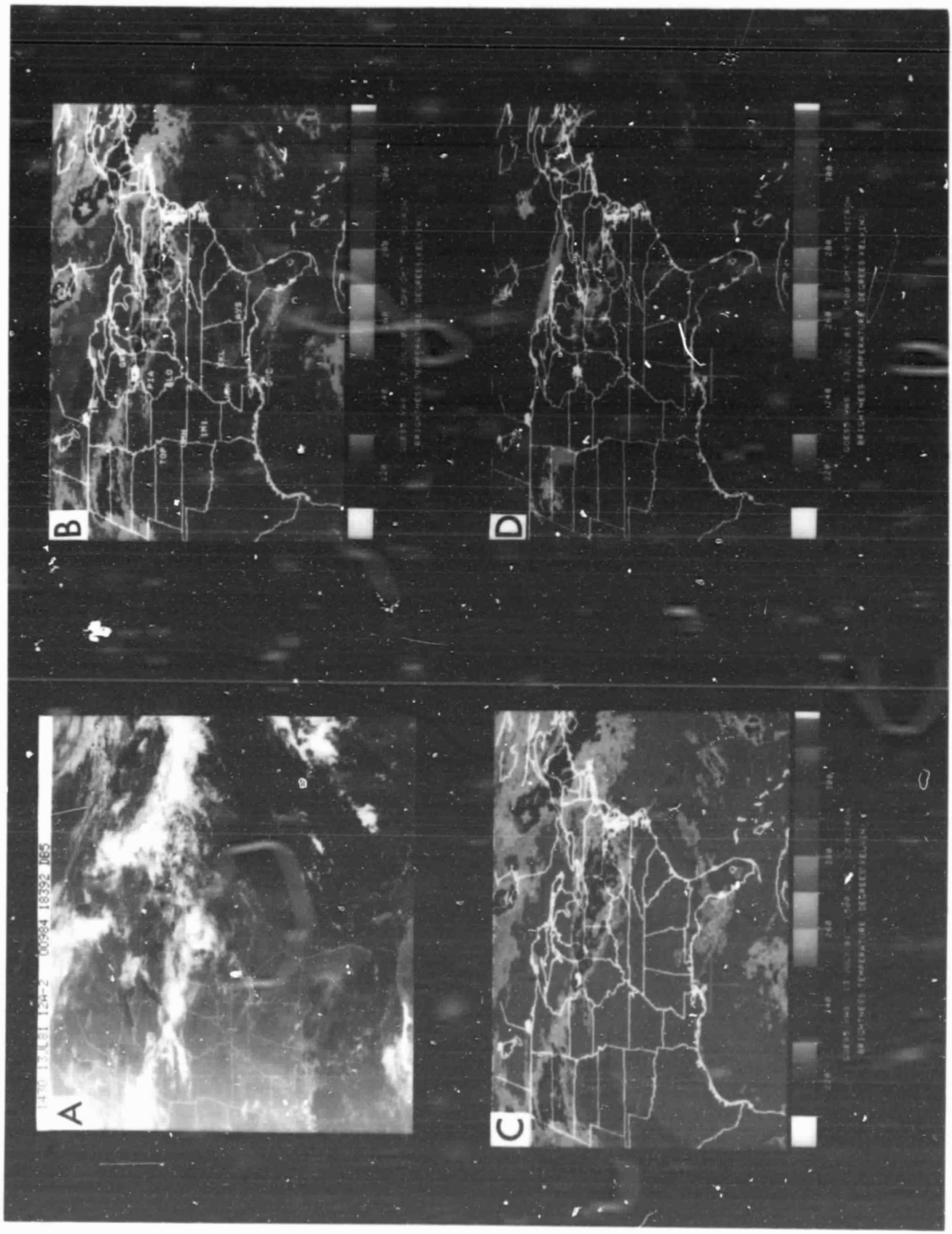

Figure 4

PRECEDING PAGE BLANK NOT FILMED

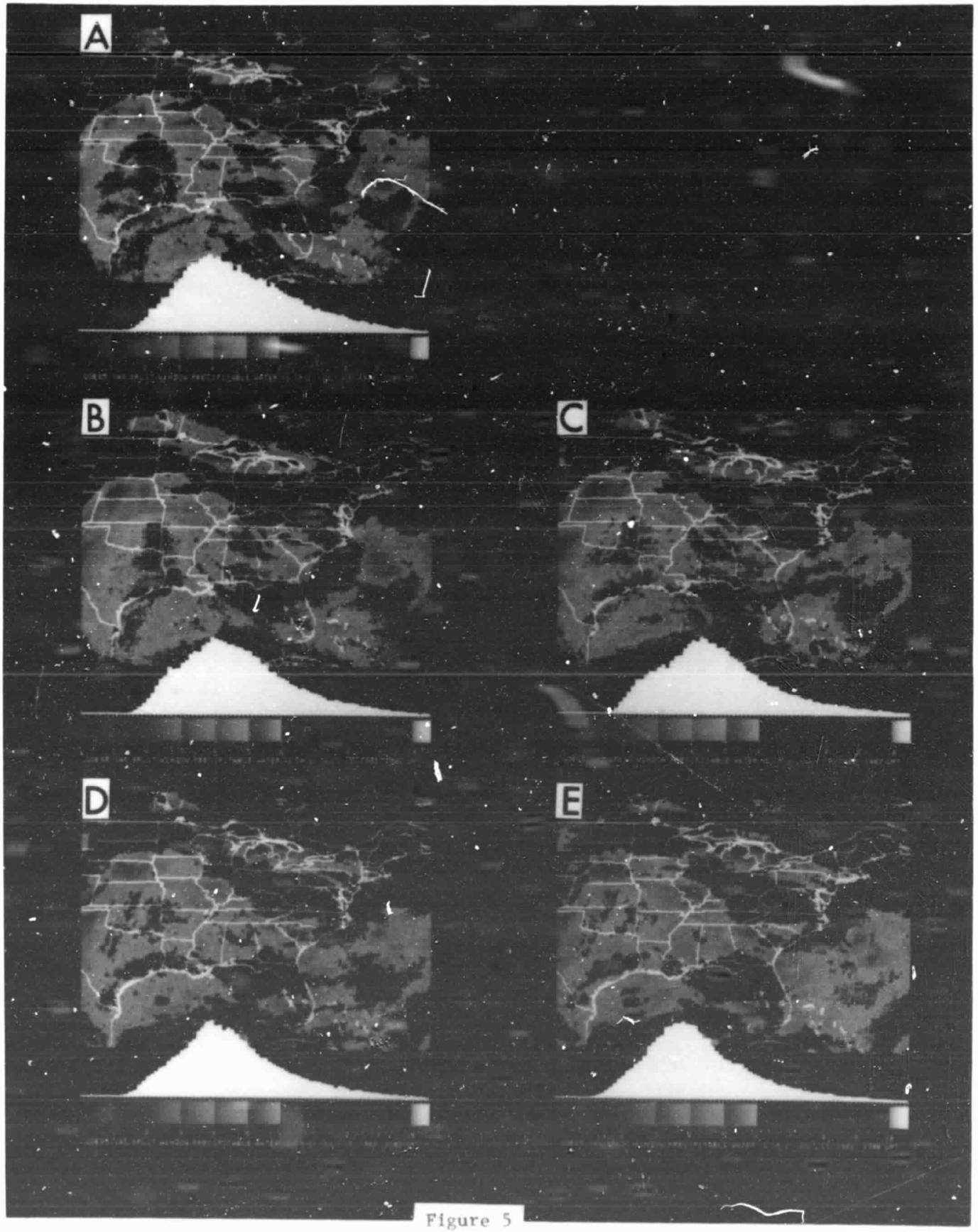

Figure 5

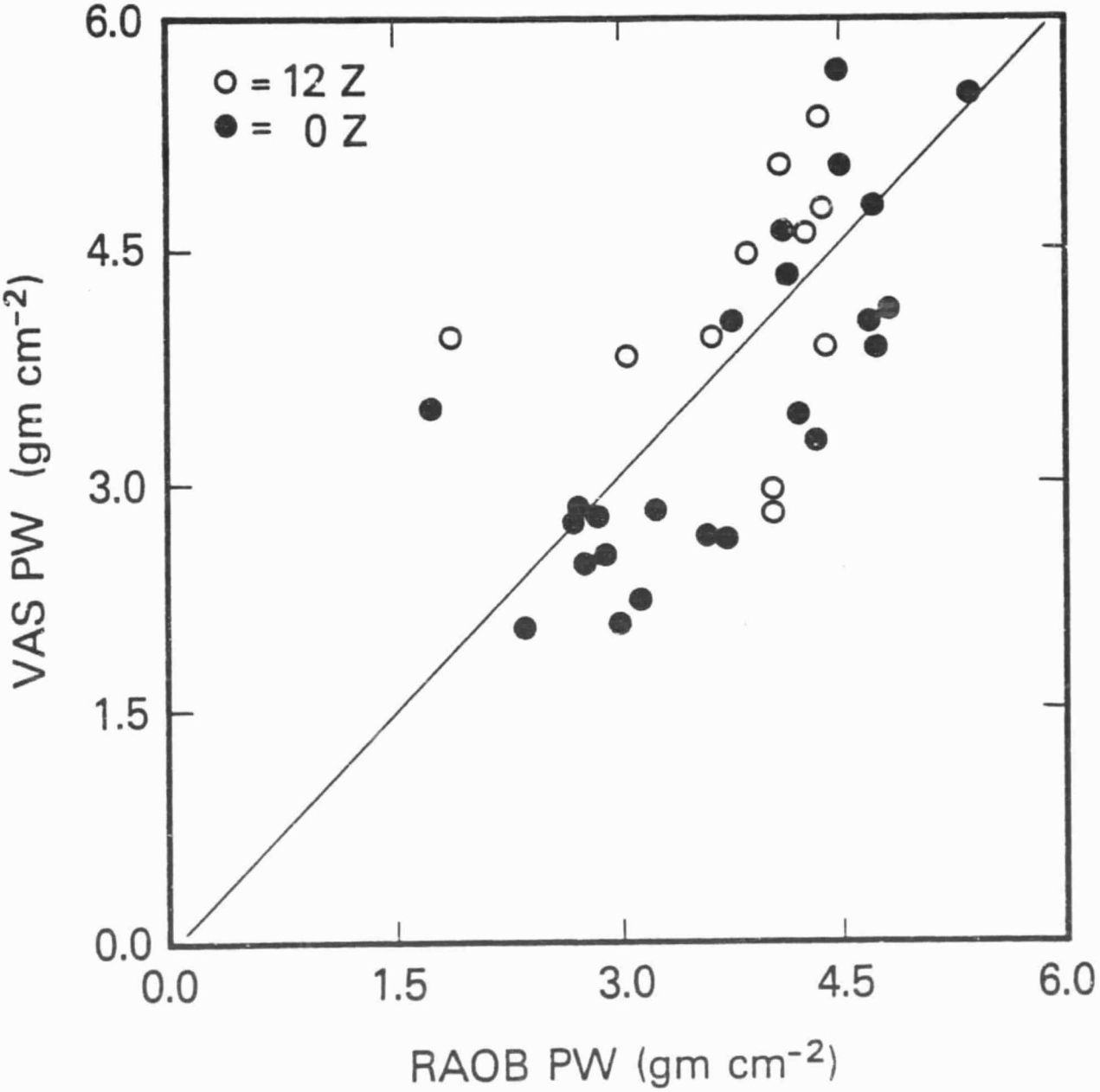

Figure 6.